Time-dependent diffusion in stellar atmospheres

Georges Alecian, Martin J. Stift, E. A. Dorfi

Monthly Notices
of the
ROYAL ASTRONOMICAL SOCIETY

Mon. Not. R. Astron. Soc. **418,** 986–997 (2011) doi:10.1111/j.1365-2966.2011.19547.x

Time-dependent diffusion in stellar atmospheres

G. Alecian,[1⋆] M. J. Stift[1,2] and E. A. Dorfi[2]

[1]*LUTH, Observatoire de Paris, CNRS, Université Paris Diderot, 5 Place Jules Janssen, 92190 Meudon, France*
[2]*Institut für Astronomie (IfA), Universität Wien, Türkenschanzstrasse 17, A-1180 Wien, Austria*

Accepted 2011 August 1. Received 2011 July 29; in original form 2011 June 10

ABSTRACT

The chemical peculiarities of Ap stars are due to abundance stratifications produced by atomic diffusion in their outer layers. Theoretical models can predict such stratifications, but so far only provide equilibrium solutions which correspond to the maximum depth-dependent abundances for each element that can be supported by the radiation field. However, these stratifications are actually built up through a non-linear, time-dependent process which has never been modelled for realistic stellar atmospheres.

Here, we present the first numerical simulations of time-dependent diffusion. We solve the continuity equation after having computed, as accurately as possible, atomic diffusion velocities (with and without a magnetic field) for a simplified fictitious – but still realistic – chemical element: cloudium. The direct comparison with existing observations is not the immediate aim of this work but rather a general understanding of how the stratification build-up proceeds in time and space. Our results raise serious questions as to the relevance of equilibrium solutions and reinforce the suspicion that certain accumulations of chemical elements might prove unstable.

Key words: diffusion – stars: abundances – stars: chemically peculiar.

1 INTRODUCTION

Abundance stratifications of several metals have been detected in the atmospheres of Ap-Bp stars, including HgMn stars (see e.g. Ryabchikova et al. 2002; Shulyak et al. 2009; Kochukhov, Shulyak & Ryabchikova 2009; Thiam et al. 2010). These detections could be subject to quantitative adjustments in the future, but the existence of vertical abundance inhomogeneities in the outer layers of chemically peculiar (CP) stars has to be considered well established. Such stratifications have been predicted by theoretical models invoking atomic diffusion throughout the four decades following the seminal work of Michaud (1970). Quantitative estimates of the accumulation of elements in the atmospheres of CP upper main-sequence stars atmospheres were published shortly after that pioneering article.

In recent years, theoretical studies addressing the problem of abundance stratification in stellar atmospheres have progressed significantly (Alecian & Stift 2007; LeBlanc et al. 2009), and bi-dimensional vertical distributions of metals have been computed for magnetic atmospheres by Alecian & Stift (2010). However, because detailed computations would require excessive computing resources, all these studies have only considered equilibrium solutions (see the discussion in Section 2 of Alecian & Stift 2007). Actually, the stratification build-up is a non-linear time-dependent process – so far never followed numerically for these atmospheres – and fundamental questions arise such as: do real stratifications converge with time towards equilibrium solutions, and are the real stratifications stable? Observations of Ap-Bp stars show a rather large spread of abundances, with some general trends compatible with predictions of the diffusion model. But these trends are not systematic enough to confirm that equilibrium solutions are generally reached in real systems. On the other hand, there is at least one star in which a secular evolution of mercury spots was discovered (Kochukhov et al. 2007). As discussed in Alecian & Stift (2006) at the end of their section 4.1, spots on magnetic Ap stars are due to vertical diffusion and magnetic geometry.[1] Since the timescales of horizontal diffusion exceed those of vertical diffusion by 4 to 5 orders of magnitude, horizontal diffusion can be neglected. Any detectable changes in the surface abundance inhomogeneities – such as changes in the shapes of the spots – are thus expected to be due to changes in the magnetic field geometry (unlikely for fossil fields), to changes in local mixing, or to a vertical instability of clouds built up by atomic diffusion. The secular evolution observed for mercury can probably be considered supporting evidence for the unstable abundance stratifications scenario (Alecian 1998), but the other physical processes mentioned cannot be discarded. Keep however in mind that, whatever the initial cause of these changes might

⋆E-mail: georges.alecian@obspm.fr

[1] As stated by Alecian & Stift (2010), the entire surface of an Ap star can be reasonably approximated as the juxtaposition of independent facets, computed using plane-parallel atmospheres.

be, atomic diffusion must have time enough to adjust abundances inside the clouds.

In the present study, we numerically solve the time-dependent equations for atomic diffusion in a simple case and present, for the first time, a simulation of the abundance stratification build-up in a stellar atmosphere. To make the problem tractable in terms of computing time, we have created a fictitious but realistic element, the 'cloudium', choosing its atomic properties (for instance, the number of bound–bound transitions, their strength and their wavelength) such that the computation of diffusion velocities by our code is very fast. At the present stage of the development of the code, our purpose is to improve our understanding of the process in time; we do not yet intend to quantitatively reproduce observed abundance stratifications.

In Section 2, we recall some theoretical aspects of the abundance stratification build-up and in Section 3 we describe our numerical methods and the adopted approximations. In Section 4 we present the fictitious element cloudium created for our study; we present and discuss the numerical results in Sections 5 and 6.

2 TIME-DEPENDENT BUILD-UP OF ABUNDANCE STRATIFICATIONS

In the test-particle approximation, the 1D continuity equation for a given element may be written as

$$\partial_t n + \partial_z \left[n \left(V_{\rm D} + V_{\rm M} \right) \right] = 0, \qquad (1)$$

where n is the local number density of the element in consideration and $V_{\rm D}$ its diffusion velocity (Alecian & Stift 2006); $V_{\rm M}$ is a macroscopic velocity (corresponding to a global flow of matter, e.g. a stellar wind). In the present study we consider the case with no macroscopic motion ($V_{\rm M} = 0$). In magnetic atmospheres, the diffusion velocity is no longer strictly vertical (except at the magnetic poles). However, because the vertical atomic diffusion time-scale is much shorter than the horizontal one (Alecian & Stift 2006), the plane-parallel equation (1) remains a good approximation even in the magnetic case.[2]

Equation (1) describes the abundance change with time and depth. The initial abundance can be assumed to be homogeneous; the starting time ($t = 0$) may correspond to the moment of the star's evolution when mixing processes become negligibly small with respect to diffusion processes in the layers considered. The evolution of the abundance depends on boundary conditions (see Section 3.2). Because the diffusion velocity varies by several orders of magnitude from the bottom of the atmosphere to the highest layers, we are faced with a stiff problem.

We show in Fig. 1 an example of diffusion time-scales computed by our code CARAT (using the most recent version with an extended atomic lines list). This computation was carried out in local thermodynamic equilibrium (LTE), for a non-magnetic atmosphere with $T_{\rm eff} = 12\,000$ K, $\log g = 4.0$ (ATLAS12 model; Kurucz 2005). The diffusion velocities used to estimate the time-scales presented in Fig. 1 were computed for solar abundances and thus correspond to the situation at the very beginning of the stratification process. We define the time-scale as the time needed for atoms of the species under consideration, to diffuse through a distance of 1 pressure scaleheight: when the time-scale is 1 year in some layer, we can expect a significant abundance change in that layer in about 1 year,

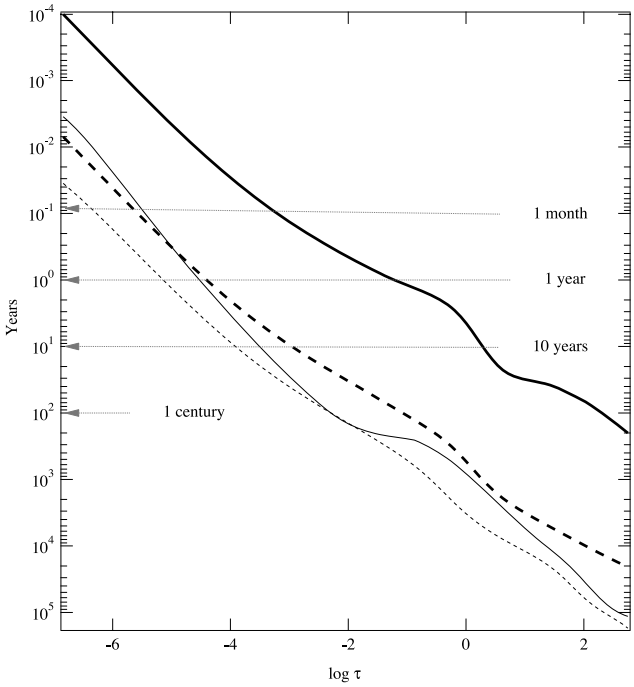

Figure 1. Diffusion time-scales for Fe and Hg [log(years) versus log(optical depth at 5000 Å)] for a non-magnetic atmosphere with $T_{\rm eff} = 12\,000$ K, $\log g = 4.0$. Note that the time-scale axis (left-hand axis) is reversed. Solid lines correspond to diffusion time-scales, and dashed lines to gravitational settling (diffusion without radiative acceleration). Heavy lines are for Hg, and the others for Fe. The higher the curves, the shorter the time-scales. In these computations, the diffusion time-scale for Hg is much shorter than for Fe; Hg abundances could change significantly in less than 1 month above $\log \tau < -4$ (see text).

since that layer can be reached by all the diffusing particles inside a column with a length of one pressure scaleheight. Of course, one cannot know quantitatively how much that abundance changes without solving equation (1). This is precisely the problem we want to address in this work. According to the time-scales of Fig. 1, significant changes in Hg abundances can be observed within just 10 years above $\tau_{5000} < 1$, while more than three centuries should be necessary for Fe. Diffusion time-scales for Hg (at solar abundance) are much shorter than for Fe because the Hg lines are far from their saturation threshold; radiative accelerations and resulting diffusion velocities thus remain large (large overabundances of Hg are required for line saturation and ensuing reduction of the radiative accelerations). In other words, this is due to the low solar abundance of Hg: momentum acquired by Hg through photo-absorption has to be shared by a much smaller number of Hg ions than is the case for Fe. This situation is often found for elements of low abundance.

Atmospheres being optically thin, the calculation of radiative accelerations requires detailed non-local radiative transfer solutions for each wavelength and time-step. Prohibitively expensive numerical computations can only be avoided for stellar interiors which have the advantage of being optically thick (see e.g. Turcotte, Richer & Michaud 1998; Seaton 1999). An early theoretical and numerical study of equation (1) was carried out by Alecian & Grappin (1984). These authors concluded that abundance stratifications due to atomic diffusion are stable in the optically thick case, but they speculated on possibly unstable stratifications in the optically thin case. Indeed, an unstable scenario was described by Alecian (1998). According to this scenario, a cloud of metal starts to form in high

[2] Horizontal abundance inhomogeneities result from the magnetic field geometry and vertical diffusion, not from horizontal diffusion.

atmospheric layers. Since the diffusion time-scale is short when the density is low, the abundance anomalies must first affect higher layers. Such an accumulation of metal could become thicker and thicker with time, with the base of the cloud propagating towards deeper layers (if the radiative acceleration is large enough). In such a case, the photon flux which supported the top of the cloud at the beginning of the process – the medium being optically thin, these photons come from deeper layers – is no more available (since the photons are absorbed by the deeper layers where the overabundance is increasing), and the cloud could collapse. One can carry the speculation further by assuming that the cloud will be reborn in a kind of cyclic process.

The feasibility of such an unstable cloud scenario for stellar atmospheres has never been verified because a complete solution of equation (1) is still out of reach. We propose in this work to solve this equation under some approximations as detailed in the following sections and for a fictitious element especially designed to allow fast computation of its diffusion velocity.

3 THE NUMERICAL CHALLENGE

3.1 Transport of atoms

The transport of a particular species with number density n is determined by the equation of continuity

$$\frac{\partial n}{\partial t} + \nabla \cdot (n\,\boldsymbol{u}) = 0\,, \tag{2}$$

where $\boldsymbol{u}$ denotes the diffusion velocity. Equation (2) assumes that no sources or sinks are modifying the number density n. In the case of a planar 1D geometry depending only on the height z in the stellar atmosphere this equation simplifies to

$$\frac{\partial n}{\partial t} + \frac{\partial (nu)}{\partial z} = 0 \tag{3}$$

which can be transformed to an optical depth scale by

$$\mathrm{d}\tau = -\kappa_{\mathrm{s}}\,\mathrm{d}z\,, \tag{4}$$

where κ_{s} is the standard continuous opacity at 5000 Å.

Since the background structure of a stellar atmosphere as well as the radiative forces are given between two optical depth points, i.e. between the lower boundary at the bottom of the atmosphere and the upper boundary (the layer with the smallest optical depth), we have to specify boundary conditions for the number density at these locations z_{low} and z_{upp}, respectively. At the bottom of our computational domain we can assume that a large reservoir of atoms is available so as to keep the number density constant, i.e.

$$n(z = z_{\mathrm{low}}) = n_0 \quad (= const.) \tag{5}$$

The validity of this condition is further strengthened in the case of small gas velocities u_0 of the order of a few $\mathrm{mm\,s^{-1}}$ at the lower boundary and if the time-span of our computations Δt is small enough to ensure

$$n_{\mathrm{loss}} = \int_{\Delta t} \dot{n}\,\mathrm{d}t \ll N_0\,, \tag{6}$$

where N_0 denotes the total number of atoms below the lower boundary available for atomic diffusion.

The upper boundary condition at the top of the atmosphere can be formulated in the case of positive outflow velocity $u \geq 0$ by assuming that no further acceleration takes place, leading to a so-called outflow boundary condition with zero gradient in the velocity

$$\left.\frac{\partial u}{\partial z}\right|_{z=z_{\mathrm{upp}}} = 0. \tag{7}$$

In the case of an inflow from outside, i.e. $u(z_{\mathrm{upp}}) < 0$, we have to stop our computations unless additional assumptions are made concerning the number density above the stellar atmosphere model.

3.2 The numerical technique

The computational domain is discretized between z_{low} and z_{upp} using N spatial grid points z_i with $1 \leq i \leq N$. The locations z_i are fixed and equally distributed in $\log\tau$, given through relation (4). Since we are interested in the long-term evolution of the number density we have to make the comparison between this evolutionary time t and the order of magnitude of the flow-time

$$t_{\mathrm{flow}} \sim \int_Z \frac{dz}{|u(z)|} \tag{8}$$

through the computational domain resulting in $t \gg t_{\mathrm{flow}}$. For this reason and in order to avoid the restrictive Courant–Friedrichs–Lewy (CFL) condition which severely limits the time-step, we choose an implicit discretization of the equation of continuity (equation 3). More details on these problems and on related numerical methods can be found in Dorfi (1998). For numerical stability reasons the species have to be advected with an up-wind method across the discrete cells. We use a conservative formulation ensuring that particle conservation is guaranteed also numerically, adopting a simple first-order advection in the so-called donor-cell or upwind difference scheme. As shown in many standard textbooks on numerical fluid dynamics (e.g. Fletcher 1988), the donor-cell scheme for transport equations is always stable for implicit – as well as explicit – methods, but displays rather dissipative properties. Physical instabilities will therefore not show up immediately.

Defining the number density at position z_i at the old time level $t^{(k)}$ by $n_i^{(k)}$ and at the new time level $t^{(k+1)}$ by $n_i^{(k+1)}$ we end up with the discrete version of the continuity equation (3)

$$\Delta z_i \left(n_i^{(k+1)} - n_i^{(k)}\right) = \delta t \left(\tilde{n}_{i+1}^{(k+1)}\,u_{i+1} - \tilde{n}_i^{(k+1)}\,u_i\right)\,, \tag{9}$$

including the time step $\delta t = t^{(k+1)} - t^{(k)}$. To complete our discretization scheme we have to specify the particle fluxes at the cell boundaries

$$\tilde{n}_i^{(k+1)} = \begin{cases} n_{i-1}^{(k+1)}, & \text{if} \quad u_i \geq 0 \\ n_i^{(k+1)}, & \text{otherwise} \end{cases}\,. \tag{10}$$

Formally, we write the advected number density $\tilde{n}^{(k+1)}$ as

$$\tilde{n}_i^{(k+1)} = \alpha_i\,n_{i-1}^{(k+1)} + (1-\alpha_i)\,n_i^{(k+1)} \tag{11}$$

with

$$\alpha_i = \begin{cases} 1, & \text{if} \quad u_i \geq 0 \\ 0, & \text{otherwise} \end{cases}\,. \tag{12}$$

Such an implicit formulation for the unknowns $n_i^{(k+1)}$ leads to a tridiagonal system of linear equations including the indices $(i-1, i, i+1)$

$$a_i n_{i-1}^{(k+1)} + b_i n_i^{(k+1)} + c_i n_{i+1}^{(k+1)} = d_i \tag{13}$$

with coefficients

$$\begin{aligned} a_i &= \delta t\,\alpha_i\,u_i \\ b_i &= \delta t\,\left[-\alpha_{i+1}\,u_{i+1} + (1-\alpha_i)\,u_i\right] + \Delta z_i \\ c_i &= -\delta t\,(1-\alpha_{i+1})\,u_{i+1} \\ d_i &= \Delta z_i\,n_i^{(k)} \end{aligned} \tag{14}$$

which can be solved by standard numerical procedures. Adopting our boundary condition we find for the innermost index ($i = 1$), cf. equation (5)

$$a_1 = 0$$
$$b_1 = \delta t\,[-\alpha_2\,u_2 + (1-\alpha_1)\,u_1] + \Delta z_1$$
$$c_1 = -\delta t(1-\alpha_2)\,u_2$$
$$d_1 = \Delta z_1\,n_1^{(k)} - \delta t\,\alpha_1\,u_1\,n_0\,. \quad (15)$$

At the outermost grid point ($i = N$) the coefficients are given according to the outflow condition of equation (7) where we have $\alpha_{i+1} = \alpha_i = 1$ and $u_N = u_{N+1}$

$$a_N = \delta t u_N$$
$$b_N = \delta t u_N + \Delta z_N$$
$$c_N = 0 \quad (16)$$

$$d_N = \Delta z_1\,n_N^{(k)}\,. \quad (17)$$

The calculation can be started with a time-step δt corresponding to a small fraction of the estimated flow time $t_{\rm flow}$ (see equation 8). It is then controlled by accuracy considerations, e.g. that the temporal variation of the number density should not exceed 20 per cent at any time-step. In the case of stationary solutions this implicit discretization allows also time-steps with $\delta t \gg t_{\rm flow}$ which guarantees among others a constant flux throughout the whole computational domain.

4 A FICTITIOUS ELEMENT: CLOUDIUM

Most of the CPU time spent on solving equation (1) is required for opacity sampling and for the formal solution of the polarized radiative transfer equation needed to determine radiative accelerations. For this purpose, CaratMotion uses the same subprograms as CaratStrat (Alecian & Stift 2007). When parallel computing with p cores starts, the code divides the wavelength domain[3] into p intervals of equal width. Therefore, we ideally wish for an element whose lines that contribute to the radiative acceleration are not spread over a wide wavelength range with perhaps just one line in each interval, but rather over a few tenths of Angstroms. Of course this can never be the case for real elements, especially because one has to consider several ionization states at the same time. But as at the moment we have not gone beyond the stage of investigating qualitative fundamental properties of the stratification process and the formation of metal clouds in stellar atmospheres, we decided to design a fictitious element which meets our needs as far as possible.

The spectral lines of that element which we name 'cloudium' have to meet the following requirements:

(i) the number of lines is small, however they all contribute to the radiative acceleration.

(ii) the wavelengths of all these lines lie in a narrow spectral domain, there is no blending with strong hydrogen lines.

(iii) the lines exhibit a mixture of line strengths, from very strong to very weak lines, there is no overlapping.

(iv) several ionization states are represented.

(v) the behaviour of cloudium must look as much as possible like that of a real element.

[3] The code is able to deal with several disjointed wavelength intervals.

In order not to disturb the smooth functioning of the code, cloudium must take the place of an existing element, preferably an element which does not significantly contribute to the total opacity. The most straightforward way to proceed in the design of cloudium is to transform an existing element. We chose mercury, keeping all the properties of the three first ionization states of Hg (including the neutral state) except the bound–bound transitions list (see Table A1). We checked that the new line list fulfils satisfactorily the requirements enumerated above by examining the resulting accelerations and how they behave with changes in abundance.

One is certainly entitled to ask: why use cloudium rather than simply Hg in the numerical simulations we want to carry out? This question is a priori not unjustified, Hg being an element of low abundance compared to the iron peak elements (even in HgMn stars), so that very few of its lines (only the strongest ones) contribute significantly to the radiative acceleration. In addition, as pointed out in footnote (3), CaratMotion can deal with disjointed wavelength intervals, which makes the numerical challenge feasible for Hg, albeit at a heavier price than for cloudium. It is, however, known at a high level of confidence that Hg diffusion is strongly affected by non-LTE effects (Proffitt et al. 1999), especially in the uppermost layers close to the boundary. Our computations, however, are being carried out under the assumption of LTE, and any result on time-dependent diffusion of Hg would thus be quite misleading, inviting the reader to carry out unwarranted and misleading comparisons with observations. On the other hand, by working with the fictitious element cloudium, we are free to build toy models, play with abundances and explore various situations according to the needs of our study. Please keep in mind that only the atomic data of cloudium are fictitious, the diffusion process itself is treated fully and as accurately as possible.

5 FIRST SIMULATION OF THE CLOUDIUM STRATIFICATION

Before presenting our numerical simulations of time-dependent diffusion, we will first have a look at the diffusion of cloudium in the classic way, as found for instance in the diffusion studies of Alecian & Stift (2007) or LeBlanc et al. (2009). This analysis, which puts the properties of cloudium into the right context, is necessary to interpret the time-dependent cases presented in Section 5.2.

5.1 Equilibrium stratification of cloudium

In a first step, we have modelled the diffusion of cloudium with the help of CaratStrat, i.e. with the same tool which we use for real elements, and looked for its equilibrium stratification. The equilibrium abundance stratification is defined as the stratification that leads to zero diffusion velocities throughout the stellar atmosphere (see section 2.2 of Alecian & Stift 2007). In view of our usual approximations, this means that the radiative accelerations have exactly the same value as the gravitational acceleration, but with opposite sign; therefore this stratification corresponds to the maximum abundance which can be supported by the radiation field in each atmospheric layer. Equilibrium stratifications are obtained through an iterative process, not by integrating the time-dependent continuity equation. Fig. 2 shows the populations of the cloudium ions and the total radiative accelerations (equation 13 of Alecian & Stift 2006) corresponding to our standard homogeneous abundance. We have chosen this standard abundance to be equal to the solar abundance of mercury [1.13 on the $\log(N_X/N_H) + 12$ scale, used as the initial value for the time-dependent simulations discussed in the following

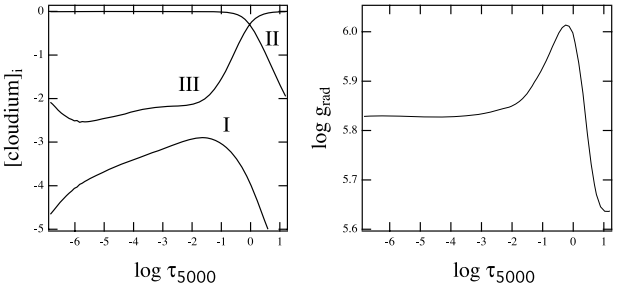

Figure 2. Left-hand panel: relative populations of the cloudium ions in LTE versus optical depth (in dex). The curve labelled 'I' corresponds to the neutral state. Right-hand panel: total radiative accelerations (zero magnetic field case) of cloudium for the standard homogeneous abundance (solar value for Hg) used as starting value in our numerical simulations (see Fig. 4).

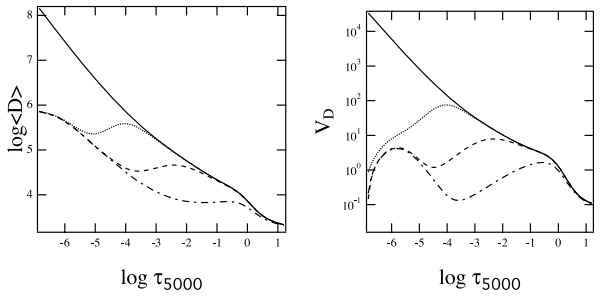

Figure 3. Left-hand panel: the cloudium diffusion coefficient (log cgs) versus optical depth. The solid line corresponds to 0 G, the dotted line to 100 G, the dashed line to 1000 G, and the dash–dotted line to 7000 G. Magnetic field lines are assumed to run horizontally. Right-hand panel: the corresponding diffusion velocities (cm s^{-1}, on a logarithmic scale), same legend as for the left-hand panel. These velocities are computed for our standard homogeneous abundance (solar value for Hg).

sections]. The accelerations shown in Fig. 2 are the accelerations at the start of the iterations. Notice that, for the initial homogeneous abundance, the radiative accelerations of cloudium exceed gravity ($\log g = 4.0$) throughout the atmosphere. This implies that the corresponding diffusion velocities are positive. The fact that the diffusion velocities are positive has important consequences for our numerical simulations, and will be discussed in detail in Section 6.

In Fig. 3 we show the diffusion coefficient and the diffusion velocity (for the same initial homogeneous abundance) as a function of optical depth for various values of the magnetic field strength (the magnetic field is assumed horizontal). Notice that even a very weak magnetic field can have a strong impact on diffusion by greatly reducing the diffusion velocity, provided that one goes sufficiently high up in the atmosphere. For horizontal field lines of only 100 G, we can see a conspicuous drop in the diffusion velocity above $\log \tau = -4$. But in spite of this drop, diffusion velocities are never close enough to zero to completely prevent diffusion because the neutral state is always present (from the point of view of diffusion, it is insensitive to the magnetic field).

Equilibrium stratifications of our fictitious element cloudium are shown in Fig. 4 for three values of the (horizontal) magnetic field strength, viz. 0, 1000 and 7000 G, which are also the values used in our time-dependent numerical simulations in the subsequent sections. We have also restricted the atmospheric domain in optical depth to the one used for the numerical simulations, i.e. $-4.2 < \log \tau < 1.2$. Because cloudium lines turn out to be unsaturated for the initial abundance, the iteration process converges to larger abundances (between 4 and 5 of the left axis). A 'hole' of cloudium

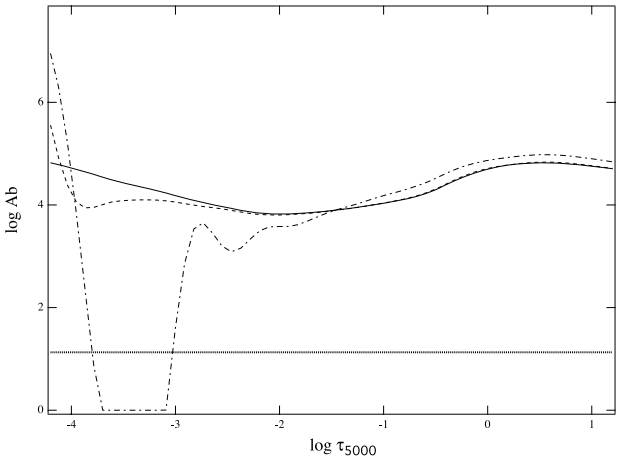

Figure 4. Equilibrium abundance stratification of cloudium [on the $\log(N_X/N_H) + 12$ scale] versus optical depth. Same legend as for Fig. 3 (the 100 G case is not shown). The horizontal grey line represents our initial standard homogeneous abundance (1.13) which is used as the starting value of the time-dependent simulations in this paper.

appears around $\log \tau \approx -3.5$ for the 7 kG case. This is due to the combination of two effects: (i) the decrease of the diffusion coefficients of the charged ions in the presence of horizontal magnetic field lines, and, (ii) the screening of the radiation field by the deeper layers (the abundance has increased in these deeper layers). The combination of these two effects results in a radiative acceleration that is always smaller than gravity in the 'hole'; there is no way for the iterative process to increase the radiative acceleration. The abundance thus unavoidably converges towards zero. Even if this scenario probably does not happen in the real-world, time-dependent diffusion process, it is, strictly speaking, not unphysical. Larger field-dependent equilibrium values of the abundance in layers deeper than $\log \tau \approx -2$ are due to the Zeeman desaturation of cloudium lines which is of course much stronger for 7 kG than for 1 kG.

5.2 Time-dependent diffusion without a magnetic field

A time-dependent simulation for the zero field case is shown in Fig. 5. This figure and the following ones are given in colour in the electronic version of the paper. The left-hand panel shows the abundance evolution [on a $\log(N_X/N_H) + 12$ scale for all the figures]; the right-hand panel gives the evolution of the diffusion flux ($n \cdot V_D$). Time-steps are very short at the beginning of the evolution (typically about a month); they increase considerably towards the end of the simulation (about 10 years for the last steps). The initial value of the cloudium abundance is constant with depth (1.13, the horizontal black heavy line of the left-hand panel). We can see in this figure that abundance starts to increase in higher layers (above $\log \tau \approx -1$) during the first 5 years. After this short phase of evolution, the abundance in these layers decreases because it is adjusting very rapidly to the decrease in flux and to the abundance decrease in deeper layers around $\log \tau \approx 0$. The main result of this simulation is that the stratification process reaches a stationary solution (constant flux throughout the atmosphere) after about five centuries of non-stationary diffusion. This solution is very far from the equilibrium solution but this does not come as a surprise: the system adjusts itself to the available flux of diffusing particles at the lower boundary (where a constant abundance is imposed; see equation 5).

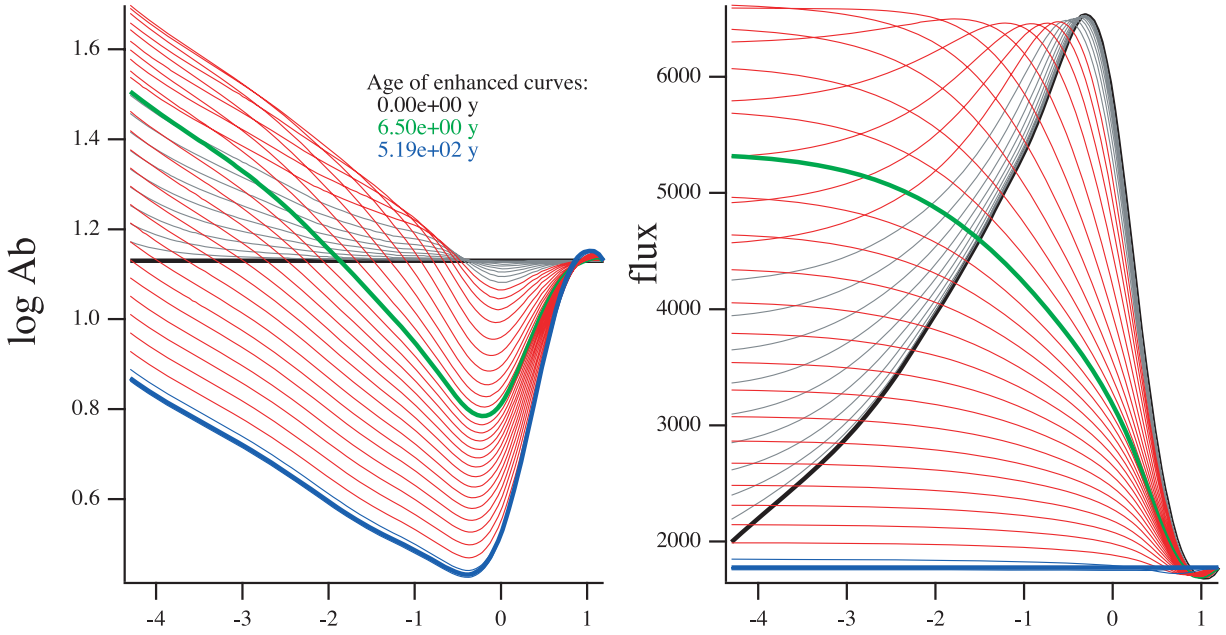

Figure 5. The zero field case. The left-hand panel shows the abundance evolution [always on a $\log(N_X/N_H) + 12$ scale] versus $\log\tau$; the right-hand panel displays the evolution of the flux (in cgs, number of particles across the unit surface per second). The initial values of abundance and flux are shown as a black heavy line, the values resulting from the next nine steps are given in grey, and the 10 final steps are in blue (most of them are superimposed in this case). Intermediate steps are plotted in red, except enhanced ones in green (one in this plot). The times (in years) corresponding to the enhanced heavy curves (black, green and blue) are given in the left-hand panel using the same colours as the respective curves. For readers having access to a grey-scale version of the figures only, notice that the horizontal line of the left-hand panel corresponds to the first step, whereas it corresponds to the last step in the right-hand panel.

According to the diffusion time-scales in the various parts of the atmosphere, the final stratification (the heavy blue curve of the left-hand panel, which corresponds to the horizontal blue line of the flux panel) adjusts continuously to the evolution of abundance deep down in the atmosphere, where diffusion induces abundance changes on much longer time-scales. In Appendix B we show the results of a simulation where the abundance is forced to change at the deepest layer (the boundary) : the adjustment is fast and smooth, the perturbed system recovers a new stationary solution in the same period of time.

5.3 Time-dependent diffusion with a magnetic field

To model time-dependent diffusion with a magnetic field is particularly important because a magnetic field is a natural barrier preventing elements from easily escaping from a stellar atmosphere. For elements like cloudium, which are subject to strong radiative accelerations in the outer layers (see Fig. 2, right-hand panel), a magnetic field should help them to accumulate in those upper layers. This is qualitatively different from the stationary solution just presented in Section 5.2 which shows no accumulation of cloudium when there is no magnetic field.

We have computed the cloudium diffusion assuming a 7 kG horizontal magnetic field. Since our code is based on the approximation of a plane-parallel atmosphere, the simulation corresponds to the cloudium diffusion at the magnetic equator. The result is shown in Fig. 6. The stationary solution is reached after about 2×10^3 years of non-stationary diffusion, a slower evolution than without magnetic field because of the smaller diffusion velocity in the magnetic case (see Fig. 3, right-hand panel). The magnetic field makes it difficult for cloudium to escape the star, and this leads, as expected, to a rather strong accumulation of cloudium above $\log\tau \approx -2$ which is even more important than the equilibrium stratification shown in Fig. 4. This is due to a somewhat lower abundance in deeper layers, which lets more photons contribute to the radiative flux, thus supporting larger cloudium overabundances than those in the equilibrium stratification discussed in Section 5.1. Looking at the left-hand panel of Fig. 6, one notes that a cloud of cloudium forms (around $\log\tau \approx -2.4$) during the first decade of diffusion. This cloud rises up in the atmosphere and reaches its maximum altitude when stationarity is achieved.

We have tried to increase the magnetic field, and have also tried to perturb this stationary solution by increasing the abundance at the lower boundary, as we did for the zero field case (Appendix B). This however led to abundances in some layers coming too close to the local equilibrium solution; diffusion velocities become negative and an instability develops (see Fig. D1). We will discuss the problem of instability in the simulations in Section 6.2.

6 DISCUSSION

We have presented simulations of the time-dependent diffusion of cloudium for two limiting cases that can be treated with the help of our code CaratMotion (in its version of 2011 May): the zero field case and the case of a 7 kG horizontal magnetic field. In addition, we have carried out simulations for some other values of the magnetic field strength (the 1 kG case is shown in Fig. C1), but we will restrict the discussion to these two limiting cases which provide typical behaviour. We stress the fact that the quantitative aspects in the following discussion depend on the properties of the

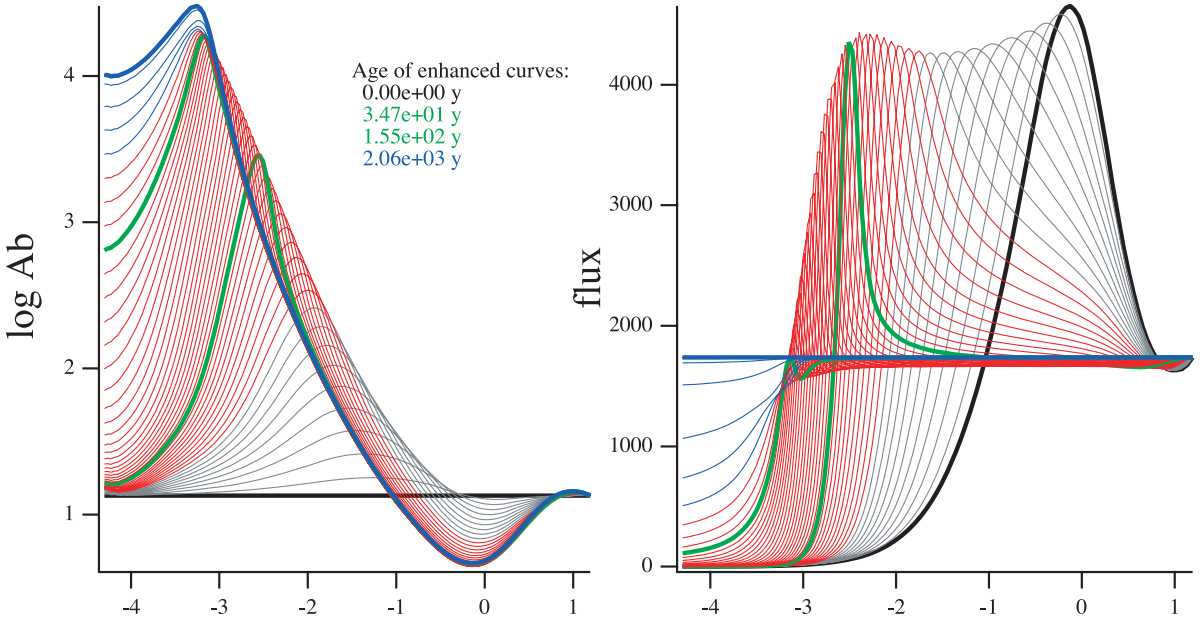

Figure 6. The 7 kG case. Same legend as in Fig. 5.

chemical element, our fictitious cloudium. However, it is possible to generalize some qualitative aspects.

6.1 The stationary solutions

In both limiting cases, a stationary solution is achieved within a short time (very short in comparison to stellar evolutionary time-scales), provided that the abundance stratification is such that the diffusion velocities remain positive (in optically thin layers; see Section 6.2) during the evolution, otherwise instabilities appear in the calculations. We chose the solar value for Hg (1.13) as initial value of the abundance for cloudium for which a stationary solution is reached (constant flux of particles throughout the atmosphere, with $V_{\rm D} > 0$) without any accumulation that would be important enough to reverse the diffusive motion of cloudium. This condition of positivity of the diffusion velocity is not met during the time-dependent evolution when the initial abundance of cloudium is too large: an instability appears before stationarity is achieved (see Section 6.2). With a magnetic field $\gtrsim$7 kG, even a small initial abundance leads to large overabundances in the upper layers in the course of evolution, and thence to instability.

In agreement with the diffusion time-scales as shown in Fig. 1, the higher the layers, the faster the cloudium abundance in these layers evolves. In the presence of a magnetic field however this is no longer true for layers above a given altitude (that depends on the field strength). For instance, for the 7 kG case, the magnetic field impedes cloudium diffusion for $\log \tau \lesssim -1.5$. The magnetic field is never a perfect barrier, since an element can diffuse across the field lines in its neutral state (which is always present). Therefore, despite the magnetic field, the cloudium accumulation takes place in high layers, slowly but unavoidably, until the flux of the escaping element balances the incoming flux at the lower boundary (i.e. the stationary solution). The slowing down of diffusion due to a magnetic field leads to larger accumulations in the upper layers since for the same particle flux, a higher abundance is needed to compensate for the smaller velocity.

In all these cases, the global shape of the final stratification of cloudium is far from the equilibrium one of Fig. 4. In fact, the stratification profile is determined by the cloudium abundance at the lower boundary. Recall that our lower boundary condition consists in keeping this abundance constant. This is physically equivalent to assume that there is an 'infinite' mixing zone below that lower boundary which maintains a constant abundance (an infinite reservoir). In real Ap stars, because diffusion proceeds also below the limits of our atmosphere, the abundance at the lower boundary will change during the star's lifetime. Because diffusion time-scales are quite short in the atmosphere (less than a century for cloudium), the atmospheric stationary solution of the element will permanently adjust itself to the abundance change at the lower boundary. This is illustrated by the experiment shown in Appendix B, where we have forced a change of abundance at the lower boundary. The system relaxes to a new stationary solution in more or less the same period of time that was needed to achieve the stationary solution starting from the initial homogeneous standard abundance (1.13), i.e. a few centuries. We have also carried out an additional experiment consisting in taking this new solution, but forcing the abundance at the lower boundary to take its initial value of 1.13. The stratification returns exactly to the previous stationary solution. This shows that, in the case of cloudium with a low abundance implying spectral lines that are almost completely unsaturated, stationary solutions are only determined by the abundance at the lower boundary.

A note of caution: one cannot be sure that the same behaviour will be observed in elements with saturated spectral lines, as for instance the iron peak elements at solar abundance. When the abundances are very small (as for the initial standard abundance of cloudium) and especially when the medium is optically thin, the radiative accelerations depend only slightly on the local abundance. But when lines are saturated and the medium is optically thick at the wavelengths considered, radiative accelerations depend non-linearly on the local abundance. This is an additional complexity which we could not fully consider in our simulations.

6.2 The unstable cases

As mentioned previously, all the simulations we carried out proved stable and smooth provided that the diffusion velocities remained

positive (upward diffusion). This limitation cannot be considered as a numerical shortcoming of the code which restricts its application to certain parameter values (see the discussion in the second part of this section). Indeed, the change in sign of the velocity has a deep physical meaning; it corresponds to a qualitative change in the diffusion regime. When the local abundance of an element increases, the radiative acceleration decreases in a non-linear way (see e.g. Alecian & LeBlanc 2000 for a general discussion of radiative accelerations). The sign of the diffusion velocity changes as soon as the outwards directed radiative acceleration becomes smaller than the inwards directed gravity. Therefore, both diffusion velocity and particle flux go through a singularity, but not the radiative acceleration. In the optically thick case, the velocity is positive for the local abundance $n < n_{\rm eq}$, and negative for the local abundance $n > n_{\rm eq}$. Therefore, there is a feedback of the system when the abundance varies about the equilibrium value[4] ($n_{\rm eq}$). In the optically thin case, instead, the radiative acceleration does not only depend on the local abundance (except perhaps in the lines core), because the absorbed photons come mainly from deeper layers; in this case, there is no local feedback to help the system to easily find an equilibrium. This lack of local feedback of the system is related to the instability mechanism recalled in Section 2, both the numerical instability and the unstable scenario being the physical consequence of the transparency of the atmosphere. Therefore, even though this has not yet been demonstrated in a rigorous way, we are inclined to consider that the numerical instability encountered by the code marks the start of a qualitative change in the diffusion regime.

To verify more quantitatively our hypothesis concerning the particular sensitivity of the stratification build-up in optically thin media, we have tried to explore the behaviour of CaratMotion with respect to a change of the sign of the diffusion velocities in the optically thick part of the atmosphere. This is meant to answer the following question: do the computation develop the same kind of instability in optically thick layers as it does in optically thin ones (see Fig. D1)? From the equilibrium abundances of cloudium shown in Fig. 4 we can define, for each layer deeper than $\log\tau = 0$, a limiting abundance above which the diffusion velocity becomes negative. In order to obtain negative diffusion velocities without provoking an unstable case as discussed above, we modified the equilibrium stratification so as to exhibit a bump with a Gaussian shape around $\log\tau = 0.5$. At the same time we avoided a high abundance at the lower boundary, thus preventing the incoming flux of diffusing particles to be too large (remember the special role of the lower boundary in the evolution of stratifications). In addition, we chose a zero field scenario to prevent cloudium accumulation in the upper parts of the atmosphere. The maximum of the bump lies higher than the local equilibrium abundance, which guarantees negative velocities around $\log\tau = 0.5$. The remaining stratification curve was taken from the stationary solution shown in Fig. 5, with some positive offset to reduce the large gradients around the bump.

The result is shown in Fig. 7 where the panels to the left show the abundance evolution, and the panels to the right the corresponding diffusion velocities. For the sake of clarity, we have divided the simulation into two parts: the upper panels display the results from the initial step to $t = 190$ years, and the lower panels give the continuation until the end of the simulation ($t = 442$ yr). The initial bump is well visible in the upper-left panel (at $\log\tau = 0.5$), and in the right-hand panel one can see that the velocity is negative around the position of the bump maximum (due to the logarithmic scale, negative velocities do not appear in the plot). From the lower panels, it emerges that the evolution leads to a new region with negative velocities around $\log\tau = -0.5$, a region where the medium is marginally optically thick. However, even though the stratification starts to show some peaks, the computation is not yet unstable in the way presented in the Appendix (see Fig. D1). The bump being rather deep in the atmosphere, the evolution is much slower than in the simulations discussed in Section 5 and a stationary solution is not reached within the 442 years covered by our run. The results show that our numerical scheme can deal appropriately with coexisting positive and negative velocities; wildly unstable solutions seem to be absent when negative velocities occur in layers where the medium is optically thick.

[4] The equilibrium value is specific to each element; it depends on its atomic properties and local plasma conditions.

7 CONCLUSION

The numerical simulations presented in this article successfully tackle the longstanding problem of time-dependent diffusion in stellar atmospheres by greatly reducing the CPU time requirements. Our approach consists in the accurate computation of atomic diffusion velocities (taking duly into account magnetic fields and detailed background opacities of the medium), that are based on a fictitious element ('cloudium') whose spectral lines have been chosen in a way as to allow fast calculations with our numerical codes while largely retaining the diffusive properties of mercury. We do not intend to analyse actual observations of a given star, but our results make it possible to understand some of the complexity of the physical processes in play during the build-up of abundance stratifications in optically thin media. They give a first glimpse of the exciting findings which can be expected from the modelling of hot CP stars.

Because the diffusion velocities strongly depend on the atomic properties of the chemical elements, the results we obtain for cloudium cannot be applied in a straightforward manner to existing observations; we are also as yet limited to cases where abundances remain low enough throughout the optically thin part of the atmosphere in order to obtain stationary solutions and to avoid the coexistence of positive and negative diffusion velocities. However, interesting qualitative behaviour is found in these numerical simulations which reveal that stationary solutions are attained on short evolution time-scales (some centuries) and that these solutions are stable as long as the diffusion velocities are positive in the optically thin layers.

When a magnetic field is present, there is always a height in the upper stellar atmosphere beyond which an element can hardly diffuse and escape from the star. Such a critical height exists for all field strengths, even for very weak magnetic fields of, say, some tens of Gauss, and might explain the phenomena in the highest layers of HgMn stars if such fields are confirmed. The effect of a weak field in HgMn stars was discussed in Alecian et al. (2009). This could be related to the observations of Adelman et al. (2002), Kochukhov et al. (2005) and Hubrig et al. (2006) who have detected variations in some sparse line profiles in a few HgMn stars and interpreted them in terms of abundance spots. The field could be largely unorganized (compared to magnetic Ap stars). Magnetic fields weaker than 10 G are still interesting in that context, even if they go observationally undetected, because they could explain spots high up in the atmosphere such as Y, Pt, Zr spots above $\log\tau = -5$. The rule is: the weaker the magnetic field, the higher up in the atmosphere such spots would form. This will work for

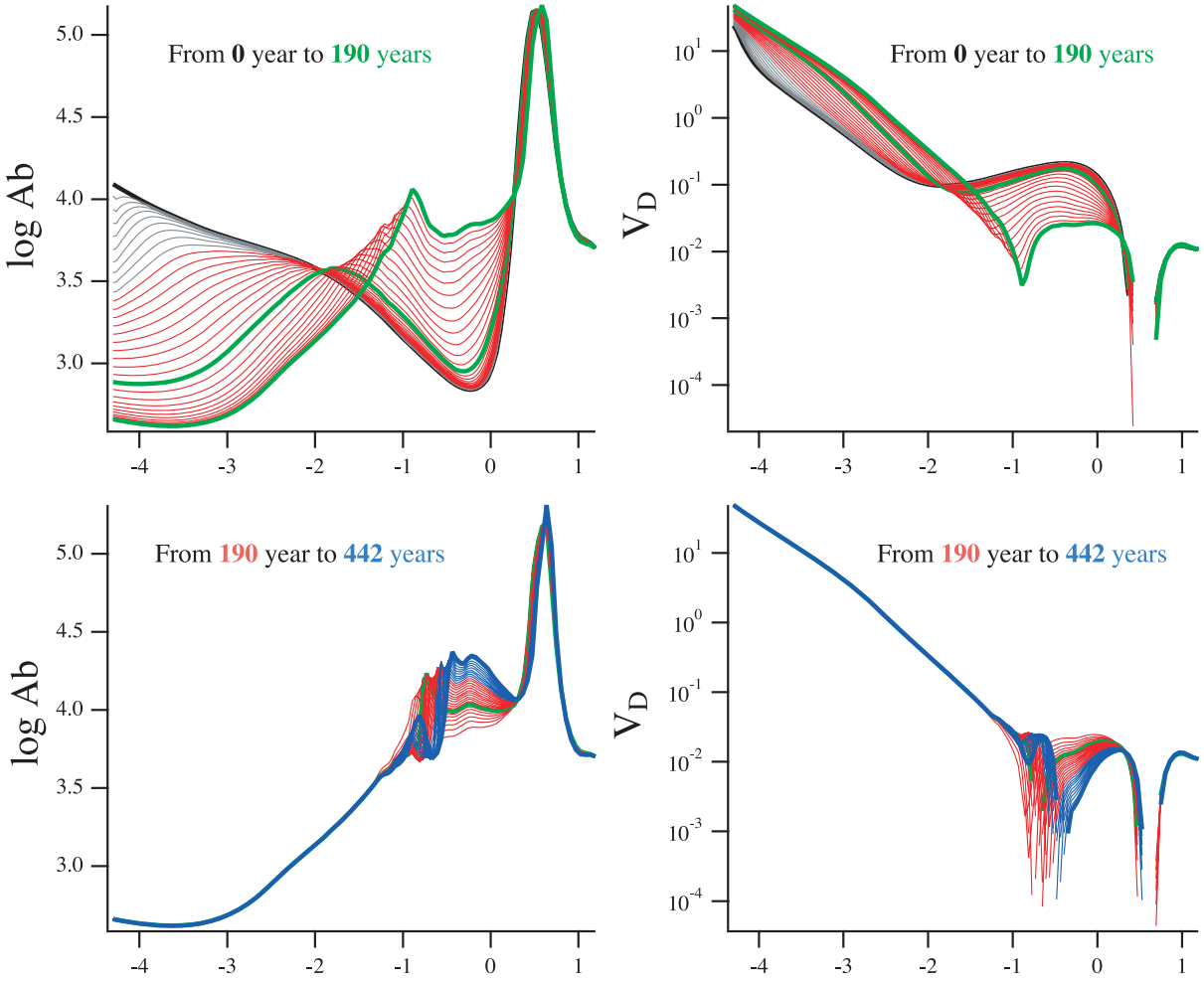

Figure 7. A zero field case, but with a hand-crafted initial stratification to explore the role of negative diffusion velocities in the optically thick part of the atmosphere. Same legend as in Fig. 5. The right-hand panels show diffusion velocities, not fluxes as in the previous figures.

elements of very low abundance (such as rare earth elements) but not for iron peak elements, to cite an example. Abundant elements should be stratified uniformly over the surface in deeper layers (e.g. $\log\tau \gtrsim -4$ for HgMn stars) where weak magnetic fields cannot affect diffusion.

Near the critical height of a given chemical element, a cloud is formed, with position, shape and concentration depending on field strength and orientation, and on the atomic properties. When the concentration inside the cloud approaches the equilibrium abundance, our numerical simulations encounter an instability and fail to further follow the evolution. We strongly suspect that, in the optically thin case, this numerical barrier marks the start of a physical instability of the stratification. This instability develops locally very steep gradients, like abundance discontinuities, which may propagate at small speeds (diffusion velocities) towards lower lying layers; note however that we solve only a continuity equation (3) for the cloudium concentration, without calculating the velocities from the Euler equation of hydrodynamics. The process we propose solely involves atomic diffusion inside a radiation flux.

Many spectral lines of a number of metals, especially the iron peak elements, are heavily saturated even when solar abundances are assumed. For these elements, no magnetic field is required to prevent them from easily escaping the star; their stratification build-up will proceed right from the beginning near the equilibrium values, both for magnetic Ap stars and for HgMn stars. We suspect that the same instability as in the cloudium case will develop if the cloud formation takes place in higher layers (we think of $\log\tau \lesssim -1.5$). These unstable cases cannot be addressed with the present version of our code and will require modifications to physics and numerics yet to be analysed.

ACKNOWLEDGMENTS

GA acknowledges the financial support of the Programme National de Physique Stellaire (PNPS) of CNRS/INSU, France. MJS acknowledges support through a Visiting Professorship at the Observatoire de Paris-Meudon and Université Paris Diderot (LUTH). This work was partly performed using HPC resources from GENCI- CINES (grants c2009045021, c2010045021, c2011045021). Thanks go to AdaCore for providing the GNAT GPL Edition of its Ada2005 compiler.

REFERENCES

Adelman S. J., Gulliver A. F., Kochukhov O. P., Ryabchikova T. A., 2002, ApJ, 575, 449
Alecian G., 1998, Contr. Astron. Obser. Skalnate Pleso, 27, 290
Alecian G., Grappin R., 1984, A&A, 140, 159

Alecian G., LeBlanc F., 2000, MNRAS, 319, 677
Alecian G., Stift M. J., 2006, A&A, 454, 571
Alecian G., Stift M. J., 2007, A&A, 475, 659
Alecian G., Stift M. J., 2010, A&A, 516, A53
Alecian G., Gebran M., Auvergne M., Richard O., Samadi R., Weiss W. W., Baglin A., 2009, A&A, 506, 69
Dorfi E., 1998, in Steiner O., Gautschy A., eds, Computational Methods for Astrophysical Fluid Flows, 27th Saas Fee Course. Springer, Berlin, p. 263
Fletcher C., 1988. Computational Techniques for Fluid Dynamics. Vol. I., II, Springer-Verlag, Berlin
Hubrig S., González J. F., Savanov I., Schöller M., Ageorges N., Cowley C. R., Wolff B., 2006, MNRAS, 371, 1953
Kochukhov O., Piskunov N., Sachkov M., Kudryavtsev D., 2005, A&A, 439, 1093
Kochukhov O., Adelman S. J., Gulliver A. F., Piskunov N., 2007, Nat. Phys., 3, 526
Kochukhov O., Shulyak D., Ryabchikova T., 2009, A&A, 499, 851
Kurucz R. L., 2005, Memorie della Societa Astronomica Italiana Supplement, 8, 14
LeBlanc F., Monin D., Hui-Bon-Hoa A., Hauschildt P. H., 2009, A&A, 495, 937
Michaud G., 1970, ApJ, 160, 641
Proffitt C. R., Brage T., Leckrone D. S., Wahlgren G. M., Brandt J. C., Sansonetti C. J., Reader J., Johansson S. G., 1999, ApJ, 512, 942
Ryabchikova T., Piskunov N., Kochukhov O., Tsymbal V., Mittermayer P., Weiss W. W., 2002, A&A, 384, 545
Seaton M. J., 1999, MNRAS, 307, 1008
Shulyak D., Ryabchikova T., Mashonkina L., Kochukhov O., 2009, A&A, 499, 879
Thiam M., Leblanc F., Khalack V., Wade G. A., 2010, MNRAS, 405, 1384
Turcotte S., Richer J., Michaud G., 1998, ApJ, 504, 559

APPENDIX A: CLOUDIUM PROPERTIES

To establish the atomic line list of cloudium, we replaced the original lines of mercury in an empirical way by a reduced number of lines, removing lines and changing their wavelength (see Table A1).

Table A1. The cloudium line list. The column headers have their usual meaning; eV and J are given for the lower level of the transition.

λ (Å)	ID	log gf	eV	J
2000.0	80.01	0.220	0.0	0.5
2001.0	80.00	0.061	0.0	0.0
2002.0	80.01	0.230	6.383	0.5
2003.0	80.02	−1.094	5.313	3.0
2004.0	80.02	0.051	7.241	1.0
2005.0	80.02	0.111	7.241	1.0
2006.0	80.02	0.124	5.707	2.0
2007.0	80.02	0.531	7.574	2.0
2008.0	80.02	0.065	5.707	2.0
2009.0	80.02	0.257	5.707	2.0
2011.0	80.01	−0.500	0.0	0.5
2012.0	80.02	0.170	7.574	2.0
2013.0	80.02	0.056	5.313	3.0
2014.0	80.02	0.288	5.313	3.0
2015.0	80.02	0.368	5.313	3.0
2016.0	80.00	0.470	4.667	0.0
2016.3	80.00	0.060	4.887	1.0
2017.0	80.02	0.368	5.313	3.0

APPENDIX B: CHANGING THE ABUNDANCE AT THE LOWER BOUNDARY

We have taken the stratification corresponding to the stationary solution of the zero field case (Section 5.2), forcing a sudden change of the abundance at the lower boundary. The abundance at the boundary (the last layer) was raised from 1.13 to 2.00, and the shape of this jump was smoothed using a Gaussian with respect to the layer number (with standard deviation of 3). The result is shown

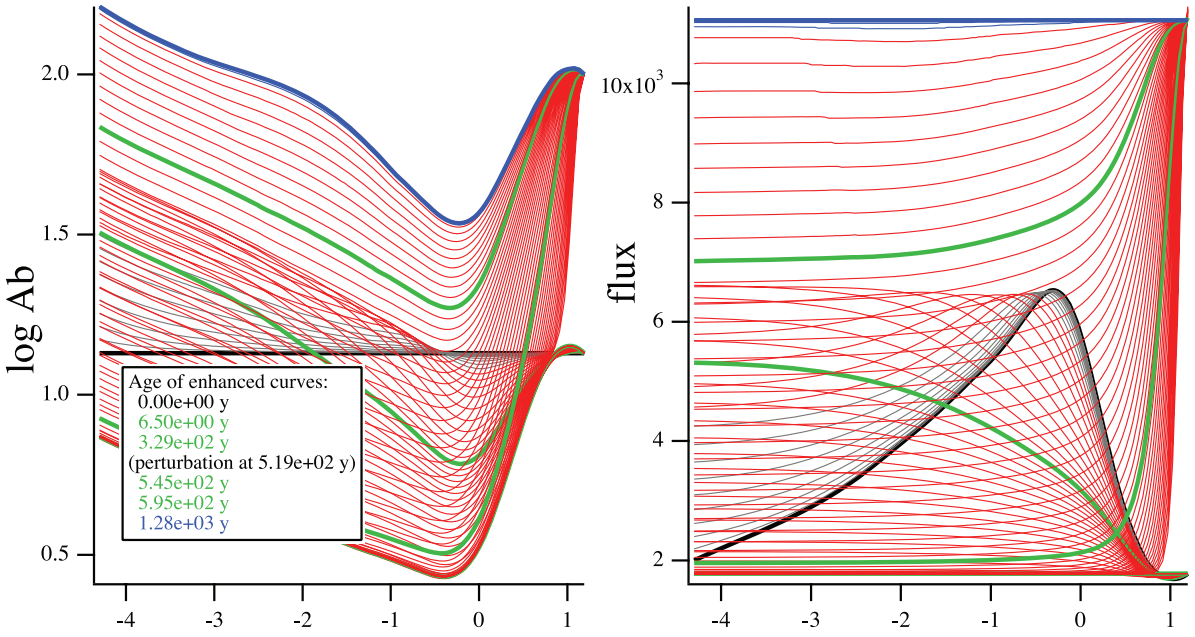

Figure B1. Perturbing the lower boundary. Same legend as in Fig. 5. This simulation starts with the same initial conditions as the one shown in Fig. 5. When the stationary solution is reached (year 519), the abundance at the lower boundary is raised to 2.00. The system evolves to a new stationary solution in about seven centuries.

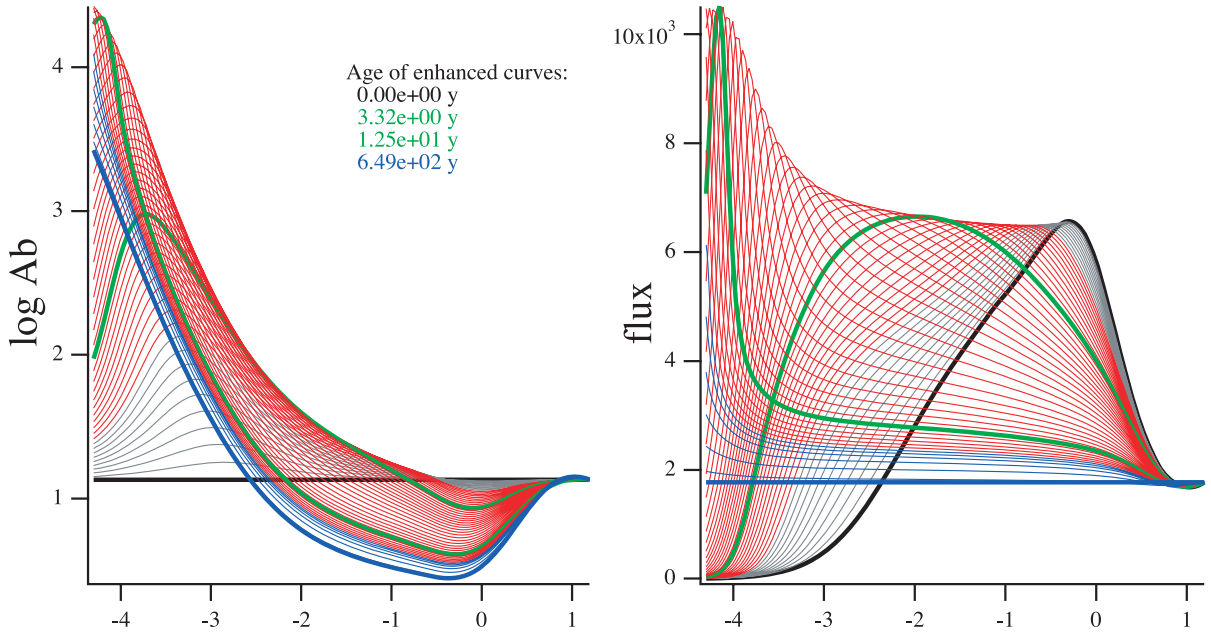

Figure C1. The 1 kG case. Same legend as in Fig. 5.

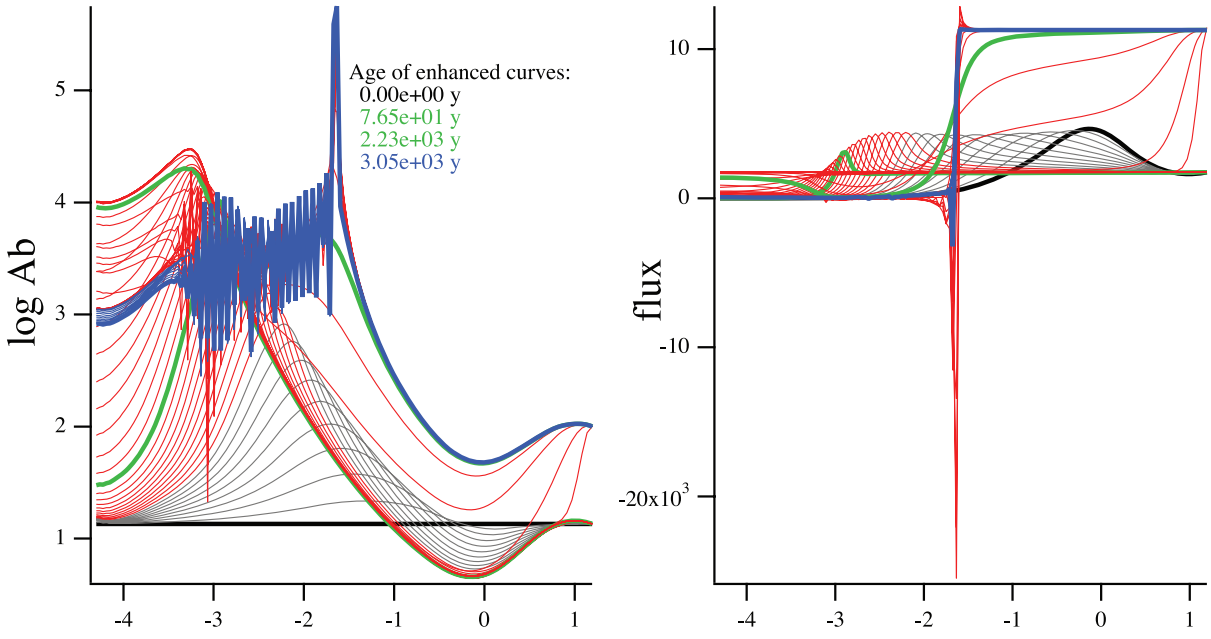

Figure D1. The 7 kG unstable case, with positive perturbation at the lower boundary. Same legend as in Fig. 5.

in Fig. B1. The system evolves smoothly towards a new stationary solution in about seven centuries.

The same experiment was carried out by reducing the abundance from 1.13 to 0.90. The system reacts in the same way and evolves towards a new stationary solution in a shorter time (about five centuries), because the cloudium lines experience less saturation than in the previous case.

APPENDIX C: 1 KG CASE

Same simulation as the one discussed in Section 5.3, but for 1 kG.

APPENDIX D: 7 KG UNSTABLE CASE

We have taken the stratification corresponding to the stationary solution of the 7 kG field case (Section 5.3), forcing a sudden change of the abundance at the lower boundary, as for the simulation shown in Appendix B. The abundance at the boundary (the last layer) was raised from 1.13 to 2.00. The result is shown in Fig. D1. It illustrates an unstable case. The abundance becomes chaotic above $\log \tau = -1.5$ where the flux reaches a sharp step shape. Evolution is virtually frozen from that final time-step.

The same experiment was carried out by reducing the abundance from 1.13 to 0.90, with the solution appearing to be stable (Fig. E1).

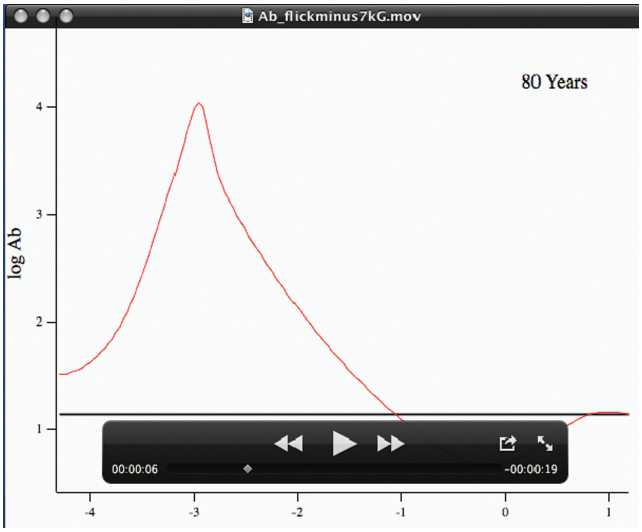

Figure E1. This animation of the abundance evolution corresponds to the case shown in Fig. 6 (7 kG), followed by a negative perturbation of the stationary solution, as the one presented in Fig. B1 for positive perturbation.

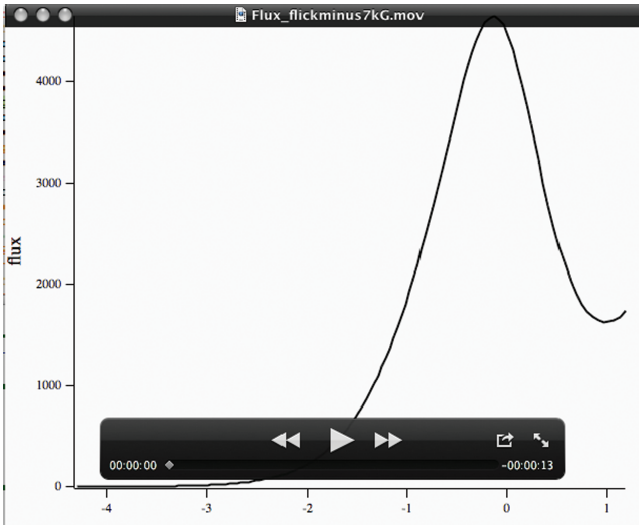

Figure E2. Same case as in Fig. E1, but for the flux (all steps are added up).

APPENDIX E: THE MOVIES

In this section, we present some of the simulations mentioned in the paper in their animated version. Original files are in.mov format and are available as online material (see Supporting Information).

List of available movies is as follows.

(i) Movie corresponding to Fig. E1. This animation of the abundance evolution corresponds to the case shown in Fig. 6 (7 kG), followed by a negative perturbation of the stationary solution, as the one presented in Fig. B1 for positive perturbation.

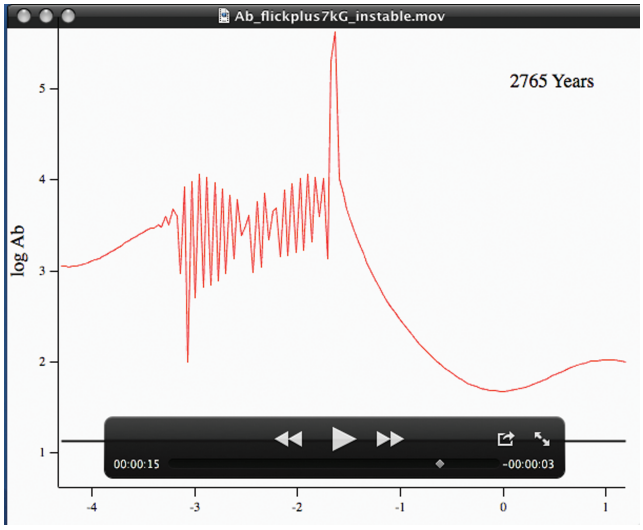

Figure E3. This animation of the abundance evolution corresponds to the case shown in Fig. D1. This case is unstable as mentioned at the end of Section 5.3.

(ii) Movie corresponding to Fig. E2. Same case as in Fig. E1, but for the flux (all steps are added up).

(iii) Movie corresponding to Fig. E3. This animation of the abundance evolution corresponds to the case shown in Fig. D1. This case is unstable as mentioned at the end of Section 5.3.

SUPPORTING INFORMATION

Additional Supporting Information may be found in the online version of this article:

Figure E1. This animation of the abundance evolution corresponds to the case shown in Fig. 6 (7 kG), followed by a negative perturbation of the stationary solution, as the one presented in Fig. B1 for positive perturbation.
Figure E2. Same case as in Fig. E1, but for the flux (all steps are added up).
Figure E3. This animation of the abundance evolution corresponds to the case shown in Fig. E1, but with a positive perturbation of the stationary solution. This case is unstable as mentioned at the end of Section 5.3.

Please note: Wiley-Blackwell are not responsible for the content or functionality of any supporting materials supplied by the authors. Any queries (other than missing material) should be directed to the corresponding author for the article.

This paper has been typeset from a TEX/LATEX file prepared by the author.